Comparative investigation of transport and deposition of nebulized particles in nasal airways following various middle turbinectomy*

Ruiping Ma[1,#], Lin Tian[2,#], Yusheng Wang[1], Siping Sun[3], Jingbin Zhang[4], Miao Lou[5], Zhenzhen Hu[1], Minjie Gong[1], Feilun Yang[1], Guoxi Zheng[1], Jingliang Dong[6,7], Ya Zhang[1]

[1] Department of Otolaryngology Head and Neck Surgery, The Second Affiliated Hospital of Xi'an Jiaotong University, Xi'an, Shaanxi, China

[2] School of Engineering, Mechanical and Automotive, RMIT University, Bundoora, VIC, Australia

[3] Zhejiang Cuize Pharmatech Co., Ltd, China

[4] Department of Medical Imaging Department, The Second Affiliated Hospital of Xi'an Jiaotong University, Xi'an, China

[5] Department of Otolaryngology Head and Neck Surgery, Shaanxi Provincial People's Hospital, Xi'an, China

[6] Institute for Sustainable Industries and Liveable Cities, Victoria University, Melbourne, Australia

[7] First Year College, Victoria University, Footscray Park Campus, Footscray, Australia

[#] contributed equally

Rhinology 62: 2, 223 - 235, 2024
https://doi.org/10.4193/Rhin23.265

***Received for publication:**
July 24, 2023
Accepted: November 12, 2023

Abstract

Background: Topical intranasal medication is required following functional endoscopic sinus surgery (FESS). The optimal particle size of transnasal nebulization aimed at the sinonasal cavities is not conclusive. The current study aims to evaluate the effect of particle size and various surgery scope of middle turbinectomy (MT) on post-full FESS drug delivery to the sinonasal cavities.

Methods: Sinonasal reconstructions were performed from post-full FESS CT scans in 6 chronic rhinosinusitis with nasal polyps (CRSwNP) patients. Four additional models representing alternative surgery scopes of MT were established from each post-FESS reconstruction for simulation data comparison. Airflow and particle deposition of nebulized delivery were simulated via computational fluid dynamics (CFD) and validated through in vitro experiments. The optimal particle sizes reaching a deposition of at least 75% of the maximum in the targeted regions were identified.

Results: The drug deposition rate onto the targeted regions increased following MT, with the greatest deposition following posterior MT (P-MT). Droplets in the range of 18-26 μm reached a deposition of larger than 75% of the maximum onto the targeted regions. Drug delivery rate in the sinonasal cavities varied significantly among individuals and across different types of MT with varying surgical scopes.

Conclusions: This study is the first to investigate the effect of various surgery scope on drug delivery by transnasal nebulization to the sinonasal cavities. The findings strongly affirm the vast potential of transnasal nebulization as an effective post-FESS treatment option. Moreover, it emphasizes that the drug delivery process via atomizers to the nasal cavity and paranasal sinuses is highly sensitive to the particle size.

Key words: transnasal nebulization, sinonasal cavities, middle turbinectomy, Computational Fluid-Particle Dynamics (CFPD), particle deposition

Introduction

The middle turbinate is a significant anatomical sign, which has a variety of physiological functions including humidification, filtration, olfaction, temperature, and airflow regulation [(1)].

Partial or complete middle turbinectomy (MT) can effectively reduce the recurrence of nasal polyps, improve the drainage of the middle meatus, and reduce nasal adhesion [(2, 3)], therefore it is widely used in patients diagnosed with chronic sinusitis with

nasal polyps (CRSwNP). However, those who favor preservation argue that MT may alter the functions of humidification and airflow regulation, lead to anosmia, ethmoid sinus scar, frontal sinusitis, and increase the incidence of postoperative bleeding [4, 5]. In addition, MT may result in the loss of anatomical landmarks, increase the difficulty of revision surgery, and increase the risk of postoperational complications [1]. Although there are various surgical methods such as complete MT, partial MT and submucosal resection in clinical practice, there is no specific guide or consensus on the effect of MT on physiological functions in functional endoscopic sinus surgery (FESS). Dayal et al. found that the volume of nasal cavity increased and nasal resistance decreased following MT via computational fluid dynamics (CFD) methodology [6], and Zhao et al. also came to the same conclusion [7]. In addition, Zhao et al. reported that there were no distinct differences in wall shear stress (WSS), airflow streamlines, and the air flux distribution between partial MT and non-resected models [7]. On the other hand, Dayal et al. found that the function of humidification and local airflow distribution were significantly altered following complete MT [6]. Friedman et al. compared the olfaction of patients pre- and post- MT and found that there was no significant change in olfactory test scores [8]. In contrast, Soler et al. found an improvement in olfaction following bilateral MT [2]. Similarly, there is no clear consensus on the deposition of drug particles in the nasal cavity following the MT.

Transnasal nebulization may overcome various patient- and drug-specific delivery barriers associated with nasal sprays, boosting the delivery to desired sites for the treatment of chronic rhinosinusitis (CRS) [9-11]. Meanwhile, most nebulizers use small particles at low velocity which are likely to travel further past the nasal valve and distribute throughout the sinonasal cavity instead of being deposited in the anterior nose [12]. Additionally, transnasal nebulization is considered a superior alternative to nasal sprays and systemic corticosteroids with respect to safety and efficacy [13, 14]. Although there are diverse nebulizer devices utilizing mechanisms such as passive diffusion, vortices, or pulsation, particle size ranges are about the same from 1-30 μm [15]. Frank et al. showed that the optimal particle size of aerosol particles via nebulization should be greater than 6.42 μm, as smaller particles may penetrate the nasal cavity and enter the lower respiratory tract [16]. Studies have reported that greater drug deposition occurred in sinuses following the surgery [17, 18], however, the ideal particle sizes of nebulizer devices for post-FESS remains unknown.

CFD simulation can obtain reliable and quantitative information and has been widely used in prediction of the deposition of inhalable particles in the nasal cavity [19, 20]. Although CFD is becoming the standard for evaluating particle deposition, there are very few CFD studies assessing the effect of transnasal nebulization. Only one study analyzed the effect of aerosolized particles in the maxillary sinus via CFD [21]. To fill the gap, current study is the first integrated numerical and experimental investigation into the effect of various surgery scopes on drug delivery by transnasal nebulization to the sinonasal cavities. Research findings are expected to identify the ideal particle size of nebulization post-FESS and serve as a foundation for achieving precision medication for middle turbinate surgery.

Materials and methods

Patient recruitment and treatment

Six patients with CRSwNP, aged 42.5±10.3 years, were recruited as volunteers in this prospective study (Table 1), according to the inclusion criteria of the Chinese guidelines for diagnosis and treatment of CRS (2018): I) Nasal obstruction, excessive nasal discharge or postnasal drip, facial pain, reduced or loss of smell for at least 12 weeks, with no improvement after regular medication treatment, and confirmed CRS through CT scans; II) Nasal polyps that affect sinus ostia or nasal sinus drainage. All subjects underwent a full bilateral FESS in all sinuses in the Second Affiliated Hospital of Xi'an Jiaotong University. All patients underwent frontal sinus dissection via agger nasi cells (Draf I / IIa) and the bilateral middle turbinate were left treated. Among them, subject 3 had a small opening of sphenoid sinus about 1.70 mm, while others were 5.02 mm in average (Table 1). To ensure a homogeneous study population, patients with septum deviation, inferior turbinate hypertrophy, polypoid middle turbinate were excluded. To simulate realistic clinical inhalation therapy practices following FESS, each subject wore a breathing mask connected to a nebulizer and underwent a fine-cut (slice thickness of 0.625 mm) dual-source siemens photon computed tomography (CT) scan from the superior edge of the frontal sinus to the level of the carina at the six-month postoperative follow-up visit. This study protocol was approved by the medical ethics committee of the Second Affiliated Hospital of Xi'an Jiaotong University (batch number: 2020-819), and all participating subjects signed a written informed consent form.

Sinonasal model construction

The CT scans were imported into Mimics imaging software to reconstruct the upper airway containing human facial features using an imaging radiation density threshold from -1024 to -300 Houndsfield (HU) to ensure an accurate anatomical structure (Figure 1A) [22]. The reconstructed postoperative models were modified in Mimics to generate four additional alternative comparative models for each subject (24 in total): I) complete MT (C-MT) - completely removal of the middle turbinate; II) posterior MT (P-MT) - removal of the posterior half of the middle turbinate; III) lateral MT (L-MT) - removal of the lateral of the middle turbinate; and IV) anterior 1/3 MT (A-MT) - removal of the anterior 1/3 of the middle turbinate (Figure 1B). Using Geomagic

Table 1. Subject demographics.

Subject	Sex	Age	History of nasal surgery	Literality of surgery	Lund-Mackay Score (Post-FESS)	Ostium of sphenoid sinus (Post-FESS)
Subject 1	M	38	0	Bilateral	2	Normal (4.36 mm)
Subject 2	F	50	0	Bilateral	4	Normal (5.87 mm)
Subject 3	M	47	0	Bilateral	2	Small (1.70 mm)
Subject 4	M	56	0	Bilateral	2	Normal (3.27 mm)
Subject 5	F	36	0	Bilateral	3	Normal (6.12 mm)
Subject 6	M	28	0	Bilateral	1	Normal (5.48 mm)

Table 2. The outlet velocity magnitudes for different subjects.

Subject	Volumetric flow rate (L/min)	Outlet area (mm^2)	Velocity magnitude (m/s)
Subject 1	15	229.81	1.09
Subject 2	15	213.78	1.17
Subject 3	15	221.13	1.13
Subject 4	15	176.06	1.42
Subject 5	15	206.61	1.21
Subject 6	15	217.39	1.15

Wrap, the three-dimensional upper airway models were divided into the vestibule, atrium, inferior meatus (inferior turbinate and its lateral wall), targeted regions (ethmoidal sinus, middle turbinate, superior turbinate, and their lateral walls), olfactory, septum, nasopharynx, laryngopharynx, tongue and maxillary sinus, sphenoid sinus and frontal sinus according to the anatomical structure (Figure 1C). Due to the highly irregular shape of the nasal cavity, bulk of the flow domain in the center is meshed with high-quality polyhedron elements with a cell dimension of 0.5 mm. A five-layer prism boundary layer of polyhedron elements with the first layer height of 0.02 mm was applied at the wall. The 3D models were meshed with a total of 2,688,312 cell elements using Fluent 19.2 (ANSYS Inc., PA, USA) (Figure 1D). A mesh preview of both the surface mesh and the interior slice mesh can be found in Figure 1D. The mesh quality was validated by ensuring the percentage of distorted low-quality elements was <0.001% [23].

Airflow and particle simulations

Se et al. and Kuprat et al. showed that most of the large microparticle deposition occurs during the inhalation phase and the equivalent steady inhalation condition does not alter the deposition results to a noticeable extent [24, 25]. Bahmanzadeh et al. conducted unsteady particle tracking of microparticle deposition in human nasal cavity under cyclic inspiratory flow condition, their results suggest that for breathing under a rest condition with a frequency of 0.25 Hz (present models also exhibit the same frequency range), the quasi-steady airflow assumption in the nasal cavity was found to be reasonable [26]. In addition, Isabey et al. have shown experimentally that the oscillatory effects are not present until Womersley number greater than 4 [27]. The Womersley number, defined as:

$$Wo_{D_h} = (D_h/2)\sqrt{(2\pi f)/v}$$

where D_h is the hydraulic diameter, f is the respiratory frequency in Hz, v is the kinematic viscosity of air ($15.1 \times 10{-}6$ m^2/s at the room temperature of 20°C) [28]. In current study, D_h for human nasal airways is 11.15×10^{-3} m. Therefore, because the normal respiratory rate ranges between 12 and 20 breaths per minute, the corresponding Wo_{D_h} is in the range of 1.27-1.64. Furthermore, experimental work by Kelly et al. and numerical simulation conducted by Keyhani et al. suggested that airflow can be considered as laminar flow up to a rate of 24 L/min [29, 30]. Therefore, in present study, an inspiratory flow of 15 L/min was used to simulate the resting state of an adult under steady-state laminar inhalation conditions. Numerical methods followed the studies of Zhao et al. and Brandon et al. [31, 32]. The entrance plane of the mask was defined as "pressure inlet" with zero gauge pressure, a temperature of 20°C (293 K), and relative humidity of 30% (absolute humidity 5.18 mg/ L). The temperature of the nasal wall was selected as 34°C (307 K) and the humidity of nasal mucosa was set at a relative humidity of 100% (absolute humidity 37.5 mg/L). The exit of the laryngopharynx was set as the "velocity outlet" of the inhaled air, with velocity calculated from the flow rate and the outlet area, at a temperature of 30°C (303 K) (Table 2) [33, 34].

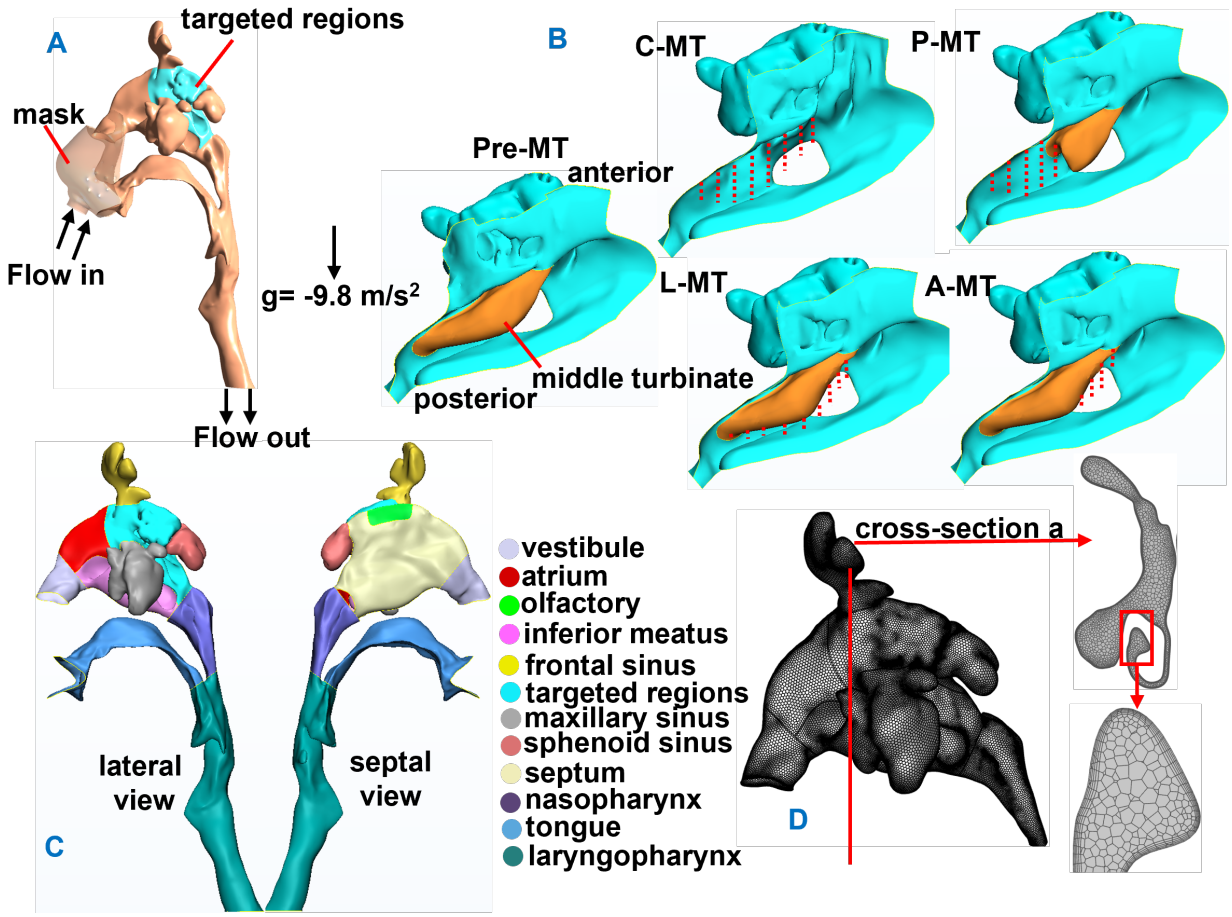

Figure 1. Sample models of subject 3: (A) Three-dimensional (3D) model of nasal cavity and paranasal sinuses. (B) Pre-MT and 4 post-full FESS virtual models (red dashed line indicates the resection). (C) Regional division of the left nasal cavity and paranasal sinuses. (D) Polyhedral mesh of upper airway models.

Incompressible Navier-Stokes equations of the viscous fluid governed the airflow motion, and the second order upwind algorithm was used to solve the governing equations. The continuity and momentum equation of the fluid flow are:

$$\frac{\partial}{\partial x_i}(\rho u_i)=0 \qquad (1)$$

$$\rho u_j \frac{\partial u_i}{\partial x_j} = -\frac{\partial p}{\partial x_i} + \frac{\partial}{\partial x_j}[\mu \frac{\partial u_i}{\partial x_j}] \qquad (2)$$

where ρ, μ and p are density, velocity, and pressure of the air, respectively. For micron-sized particles dominated by the inertial impaction, only the gravity and the drag force were considered for tracking the particles [35]. The Lagrangian particle tracking method was used where individual particle trajectories were computed. The particle equation is:

$$\frac{du_i^p}{dt} = f_D + f_G \qquad (3)$$

where the subscripts and superscript p refer to the particle phase; f_D is the drag force per unit particle mass taking the form of Stokes' drag law defined as [36]:

$$f_D = \tau_p(u_i^g - u_i^p) \qquad (4)$$

where τ_p is the particle response time, $\tau_p = 18\mu/d_p^2\rho_p C_c$; and C_c is the Cunningham correction factor to Stokes' drag law, which is calculated from:

$$C_c = 1 + \frac{2\lambda}{d_p}\left(1.257 + 0.4e^{-(1.1d_p/2\lambda)}\right) \qquad (5)$$

In this study, the direction of gravity was oriented along the negative Z-axis, suggesting a seated posture for the patient (Figure 1A). The airway wall was considered smooth and without slip.

Particle tracking was simulated using the discrete phase model (DPM) in Fluent and Lagrange tracking scheme was employed. Particles were assumed to be spherical, with density consistent with that of water. They were expected to stick to the airway

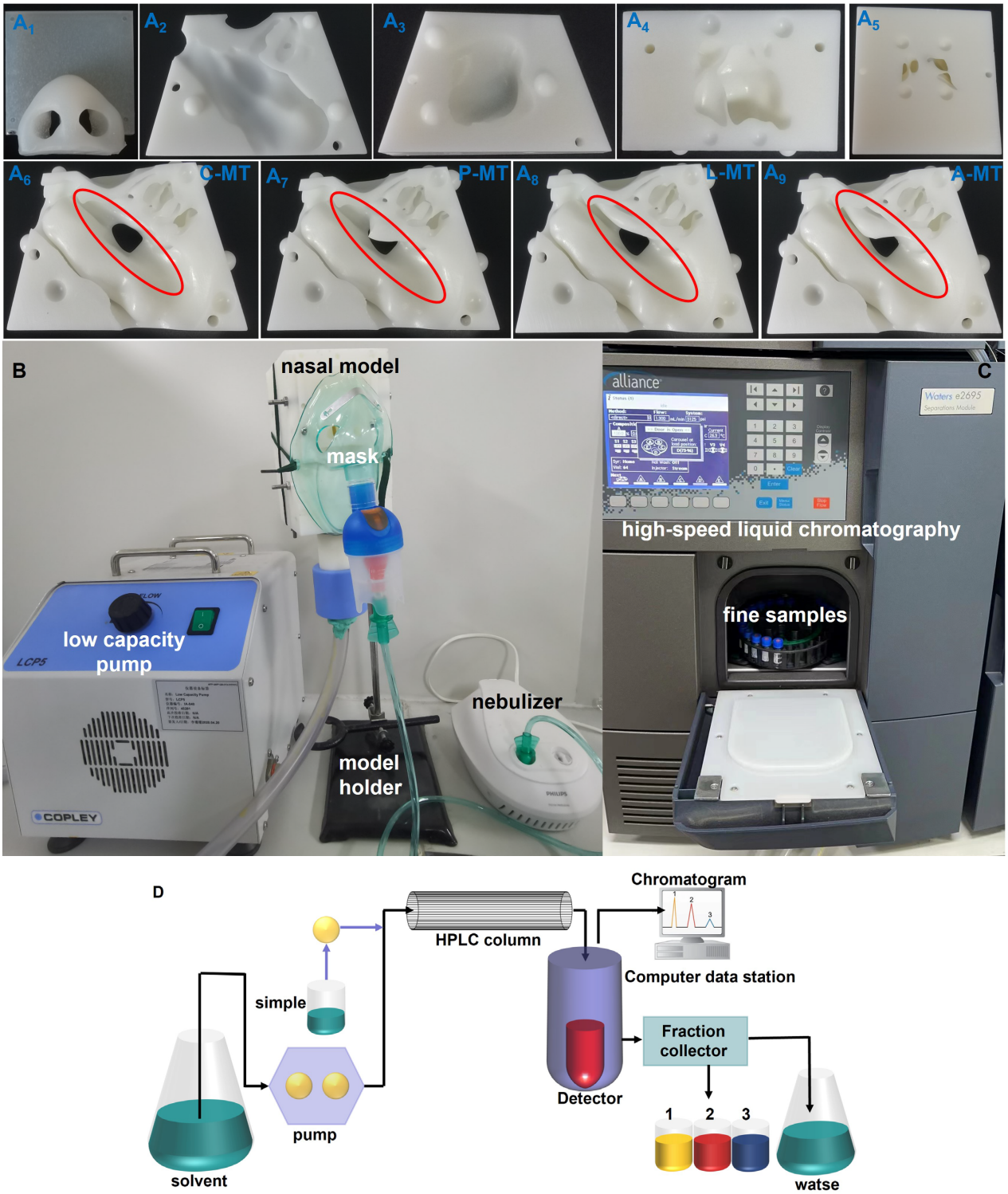

Figure 2. 3D Printed Bionic Experiment: (A) 3D printed models. (A1: vestibule; A2: septum; A3: maxillary sinus; A4: sphenoid sinus; A5: frontal sinus; A6-9: 3D printed lateral models of four post-MT. (red: middle turbinate)). (B) In vitro delivery experiment. (C) Elution and HPLC analysis of different regions for regional drug aerosol delivery. (D) Schematic diagram of HPLC.

surface upon contact, with "trapped" boundary condition. The particles arriving at the outlet were considered to pass through the upper airway, and "escaped" to the deeper airway [37]. To simulate the mask nebulized delivery, the atomization flow rate was set as 8 L/min and the velocity at the entrance of the mask was calculated from the atomization flow rate and the cross-sectional area at the inlet of the mask. 10,000 particles with the initial velocity of 0.8 m/s were uniformly released from

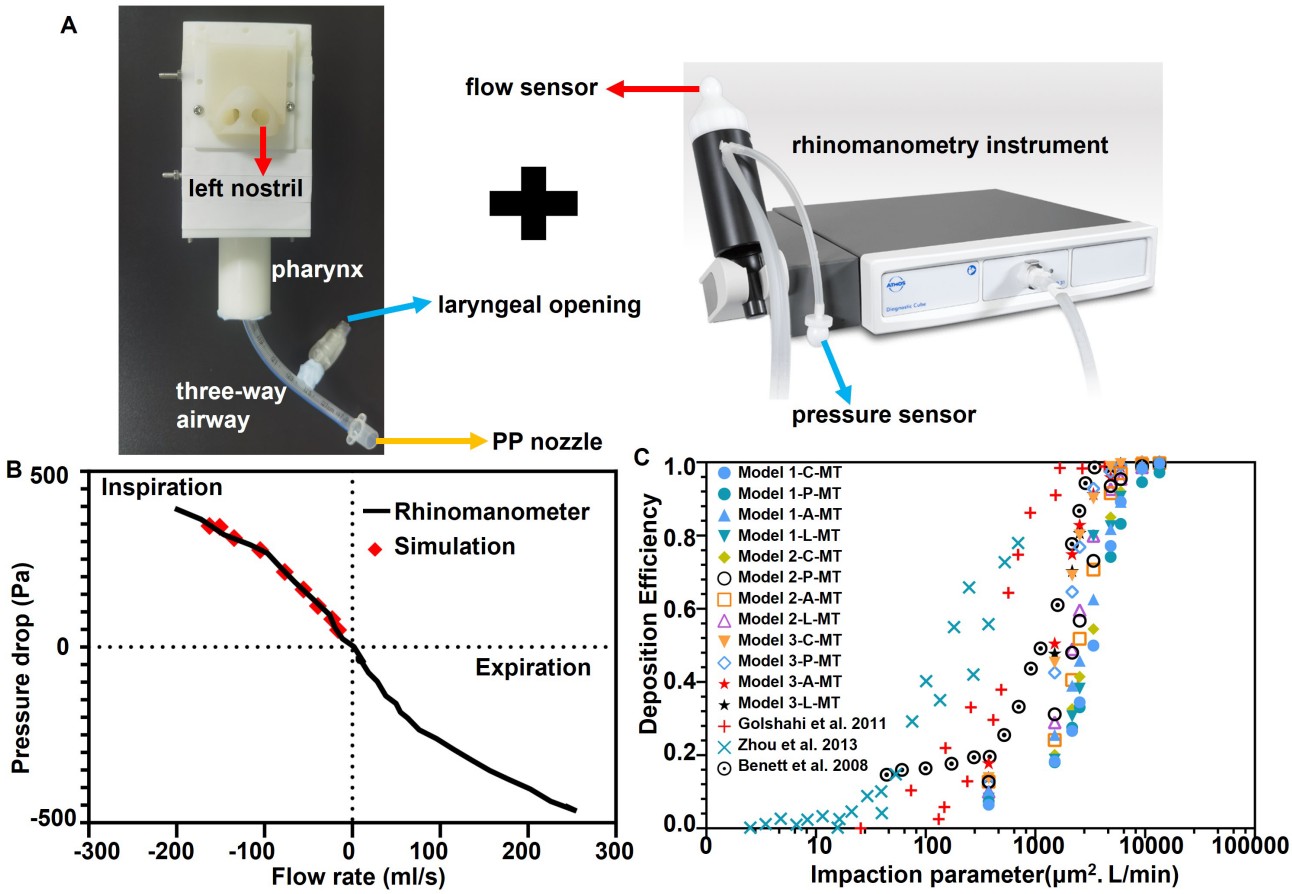

Figure 3. Model Validation: (A) Schematic diagram of nasal resistance measurement of a 3D printed model. Experimental steps: (I) the right nostril was closed, and the flow sensor is placed in the left nostril; (II) the pressure sensor is placed in the opening of the three-way airway at the throat; and (III) the experimenter breathes calmly through the PP nozzle. (B) Comparison of nasal resistances in the left nasal airway. (C) Comparison of the DE of the upper airway models.

the entrance plane of the mask. We conducted a particle size distribution analysis and found that the particle size of Budesonide atomized by nebulizer range from 1-30 μm and the mass median aerodynamic diameter was 5.75 μm. Therefore, particle deposition of 1-30 μm at 1μm increments was studied. Due to the dilute nature of the particle flow (the particle's volume fraction <0.1%), the interaction between particles is neglected, and one-way coupling between the airflow fields and the particles is assumed. The present study primarily focused on determining the initial deposition site of inhaled drug aerosols. To ensure a manageable level of research scope, the subsequent removal of deposited particles by mucociliary clearance was not considered in this work.

3D printed bionic experiment

The reconstructed nasal models were imported into 3-matic research software for segmentation according to the anatomical site. To ensure the accuracy of the models, the bilateral nasal sinuses were printed using Resin 8000 material with a strength of 56 Pa. The 3D printer, Lianruita-600 (Hangzhou Meiyi Orange Design Co. Ltd, China), features an X-Y accuracy of 0.1 mm. The nasal vestibule sections were printed with silicone to give it soft and expandable properties (Figure 2A). And to ensure the hermetic sealing of the model parts for accurate particle deposition in the sinuses, we designed sealing strips and connected each pore using screws (Figure 2B).

The following equipment was used to build the experiment rig: low-capacity pump (LCP5, IA-040), flow controller (COPLEY, DFM2000, IA-043), model holder and compressed nebulizer (Philips, CN-B-0101, 7680391), nebulized mask (Figure 2B). The mask was fixed directly in front of the model through the headband. Identically shaped filter papers were affixed to middle and inferior turbinates. Each part was coated with chromogen (SARGEL, SARTOMER ARKEMA) to facilitate the capture and collection of regional deposited particles. Budesonide (AstraZeneca Pty Ltd.,1mg) was atomized by nebulizer for 3 min, (mass median aerodynamic diameter of 5.75 μm), with a constant inspiratory flow rate of 15 L/min. After atomization was completed, each model was eluted with diluent (acetonitrile / phosphate buffer

was 35:65) in a 100 ml volumetric flask. The fine samples were analyzed by high-speed liquid chromatography (HPLC, alliance, Waters e2695, Separations Module) to obtain the deposition of each part after volumetric fixing and sampling (Figure 2C). The specific details of HPLC operation were shown in Figure 2D. Finally, the cleaning and drying models were standardized.

Visualization and statistical analysis

Visualization and analysis of the simulation results were performed using CFD-POST and Tecplot. Deposition efficiency (DE) was defined as the ratio of the number of particles deposited in a local region and the total number of particles released. The atomized particle sizes reaching a deposition of larger than 75% of the maximum in the targeted regions (ethmoidal sinus, middle turbinate, superior turbinate, and their lateral walls) were selected for results analysis. Statistical analysis was performed using SPSS 21.0 and the reported numbers included Spearman's rho and p values.

Results

Validation

To justify the reliability of the numerical model, in vitro rhinomanometry measurements were conducted on subject 3 using a rhinomanometer (ATMOS MedizinTechnik, Diagnostic Cube Rhino 31) (Figure 3A) [38]. An artificial three-way airway was made and connected to the pharyngeal outlet of the 3D printed models. A flow probe was placed at the left nostril of the model to detect the flow rates in the left nasal cavity, and a pressure probe was placed at the three-way opening of the throat to measure the transnasal pressure. The experimenter breathed calmly through the PP nozzle of the three-way tube when the contralateral nostril was closed. Then the rhinomanometry readings of the pressure drop in the nasal models were compared with the CFD data at various breathing rates, and good agreement was achieved (Figure 3B). Therefore, the CFD model is validated and can be used for further airflow analysis.

According to the particle inertia parameter: $I = Qd_{ae}^{2}$, among which d_{ae} is the equivalent aerodynamic diameter (μm) and Q is the airflow rate (L/min). To confirm the reliability of the numerical simulation, we compared the DE of particles with aerodynamic diameters in the range from 1-30 μm in the nasal cavity at flow rates of 5-15 L/min with published data on adult (Figure 3C) [17, 39]. The predicted DE curves were S-shaped, with deposition fractions near 0% for 1-2 μm particles, increasing sharply to near 100% for larger particles, and consistent with the trend of Schroeter and Siu et al. The trajectories of particles with large inertia (I greater than 1,000 μm^2. L/min) are greatly determined by inertial forces and tend to deviate from flow streamlines, with the deposition curve increasing sharply until DE reaches 100%. For inertia values less than 1,000 μm^2. L/min, deposition greatly depends on flow features. The differences in DE between models can be attributed to inter-subject variation of nasal structures that result in varying regional flow distribution among the nasal turbinates.

Effect of particle diameter

As displayed in Figure 4A, the deposition of particles in the upper airway at various sizes is marked in different colors. Compared with smaller inertial particles, particles of 30 μm (red) deposited mostly in the anterior part of the nasal cavity. The particle trajectories showed that smaller inertial particles rapidly passed through the nasal cavity and entered the laryngopharynx with a sharp change in the cross-sectional area. A fraction of them deposited onto the laryngopharynx wall, and others entered the lower airway rapidly. It was seen from the figure that large inertial particles of 30 μm were deposited at various sections of the nasal cavity and nasopharynx, and almost no particles entered the laryngopharynx (Figure 4B). Figure 4C shows the total DE of particles of 10 μm, 20 μm and 30 μm in different surgery scope of MT models. The results show that, across all models, the DE of particles of 10 μm in the upper airway is about 33%, while particles ≥20 μm are almost completely deposited in the upper airway. When the middle turbinate was not treated, the DE of 10 μm, 20 μm and 30 μm particles in the upper airway were (39.36 ± 15.89) %, (96.00 ± 4.46) % and (99.98 ± 0.03) %, respectively. After the resection of the middle turbinate, the DE of 10 μm and 20 μm particles in the upper airway were noticeably reduced compared with the Pre-MT models. In addition, compared the DE of upper airways with other models following MT, 10 μm particles were deposited more in the P-MT models and 20 μm particles were deposited less in the C-MT models. However, the DE of 30 μm particles had no significant change.

To determine size-dependent particle deposition in the targeted regions, Figure 4D displays the DE of particles of 1-30 μm in the targeted regions of the C-MT models. At particle diameter of 21 μm, the DE of the targeted regions reached the maximum, and the average deposition rate of all subjects was 25.44% following C-MT. The 3rd quartile (Q3), also referred to as the 75th percentile, was employed to demonstrate effective deposition. The targeted regions DE of no less than 75% of the maximum DE was assumed as effective deposition. For target drug delivery aiming the C-MT models' simulated target area, the effective particle diameters ranged between 18 μm and 26 μm (Figure 4D).

Effect of surgery scopes

Figure 5A depicts the DE in each anatomical region of the upper airway in the Pre-MT and 4 different scopes of MT. In relative to the Pre-MT models (green), the DE of particles with diameter ≤10 μm in the targeted regions, inferior meatus, nasal vestibule, nasopharynx, laryngopharynx, and nasal septum were not signi-

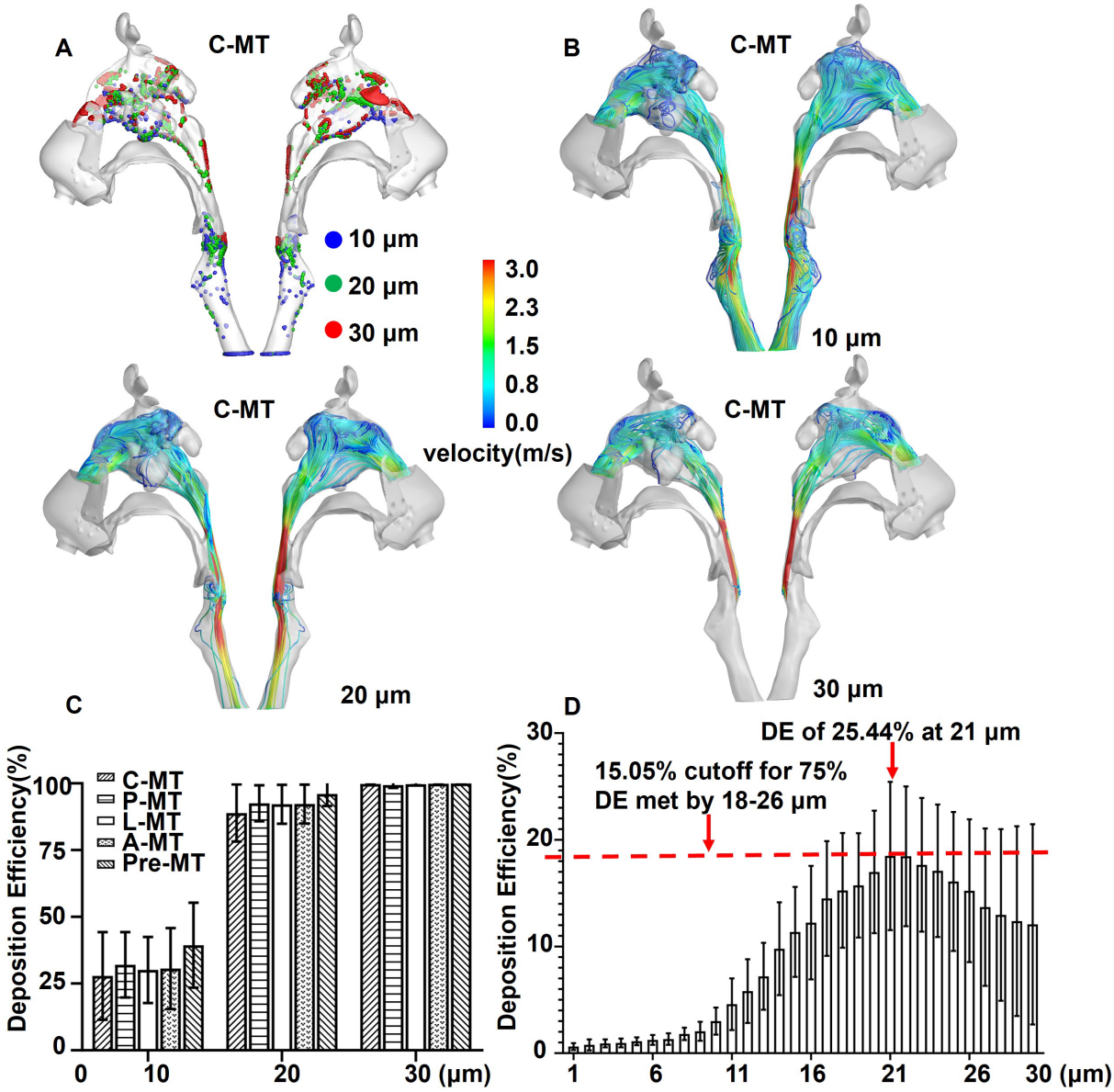

Figure 4. Deposition patterns, trajectories, and efficiency of different particle sizes in the left upper airway. (A) Deposition patterns of particles in the C-MT models at resting state. (B) Particle trajectories in the C-MT models (10, 20 and 30 μm). (C) Comparison of the deposition efficiency of particles of 10, 20 and 30 μm in respective MT models. (D) Deposition efficiency of particles (1-30 μm) in the targeted regions of the C-MT models.

ficantly different, while the DE of particles with diameter >10 μm in the various regions varied noticeably (Figure 5A, 5B). Specifically, the characteristics of the deposition rates of particles with diameter >10 μm at various sites are: I) The DE of the targeted regions increased significantly following P-MT and L-MT (especially following P-MT), while they fluctuated slightly following C-MT and A-MT (Figure 5A, 5B); II) The DE of the nasopharynx and vestibule decreased significantly following MT; and III) The DE of the inferior meatus, laryngopharynx and septum fluctuated slightly following MT.

The overall DE of particles in the range of 1-30 μm in the olfactory region was extremely low and <0.1% (Figure 5A, 5B). When the particle diameter reached 21 μm, the DE in the olfactory region increased gradually with the particle diameter in 2 of the MT models (C-MT and A-MT). There was no deposition in the rest of the MT models. The DE in the maxillary sinus, sphenoid sinus and frontal sinus varied significantly following different MT surgery scopes. The average DE in the maxillary sinus was around 1% when middle turbinate was not treated. The DE of particles with diameter ≤10 μm did not change significantly following the MT, while the DE of particles with diameter >10 μm increased distinctly, especially in the A-MT models. The average DE in the sphenoid sinus was extremely low (<0.3%) and varied significantly following various surgery scopes of MT. The different DE in the sphenoid sinus post-MT may be related to a smaller

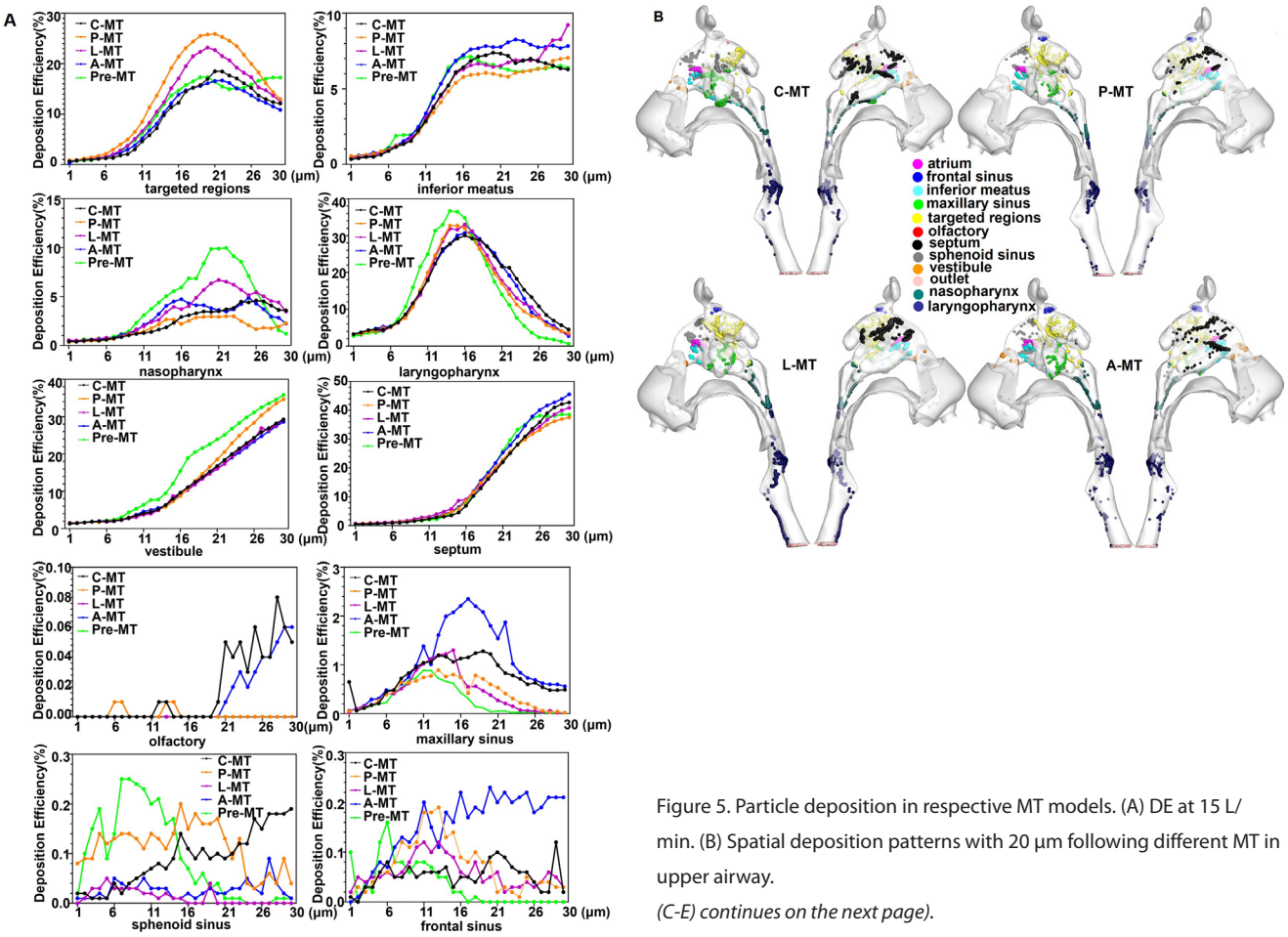

Figure 5. Particle deposition in respective MT models. (A) DE at 15 L/min. (B) Spatial deposition patterns with 20 μm following different MT in upper airway.

(C-E) continues on the next page).

opening of the sphenoid sinus in subject 3. The average DE in the frontal sinus was<0.3% and the DE of particles with diameter >10 μm increased distinctly in the A-MT models (Figure 5A, 5B).

There was no distinct difference in the the deposition pattern of budesonide in the CFD simulated and 3D printed models (Figure 5C, 5D). The particle DE of CFD and 3D printed models are shown in Figure 5E. The Spearman's rank correlation test returned R = 0.853, 0.804, 0.936 and 0.792, with the p = 0.000, 0.001, 0.000, 0.001 in the C-MT, P-MT, L-MT and A-MT models, respectively. The congruity between two ways of deposition patterns could be considered statistically significant.

Discussion

Our study investigated the increase of particle deposition rates in the paranasal sinuses by transnasal nebulization following various surgery scopes of MT, especially in the maxillary sinus. Wofford et al. reported that the average deposition rate of the nasal spray following a standard fenestration of the maxillary sinus was <1% [21], while the average DE of the maxillary sinus in the Pre-MT models was about 1%, and 1.97% post-MT in our study. In addition, transnasal nebulization appears to exhibit great efficacy of treatment and is widely distributed in the nasal cavity and paranasal sinuses. The DE of 10 μm, 20 μm and 30 μm particles in the upper airway of the Pre-MT models were (39.36 ± 15.89) %, (96.00 ± 4.46) % and (99.98 ± 0.03) %, respectively. This is consistent with the results of previous study [40]. Larger particles with 45-60 μm from conventional nasal spray devices were deposited in the nasal vault [41], whereas smaller particles from nebulization increased particle deposition beyond the anterior nasal cavity and enhanced deposition in the sinuses and posterior nasal cavity. Meanwhile, drug delivery via atomizers to the nasal cavity and paranasal sinuses is highly sensitive to the particle size and the best efficacy is obtained with 18-26 μm particles. Although two CFD studies have previously addressed the optimal particle size for nasal aerosol administration [12, 42], current study is the first to simulate the transnasal nebulization in the sinonasal cavities following MT with various surgery scope. It helps identify the ideal nebulization particle size for post-FESS treatment and provides a theoretical basis for MT.

The effect of MT on nasal physiological function has been controversial [43]. In theory, any nasal surgery can affect olfaction [44]. It was found that particle deposition in the olfactory region increased following C-MT and A-MT, which was related to the location of olfactory region in the nasal vault, superior nasal

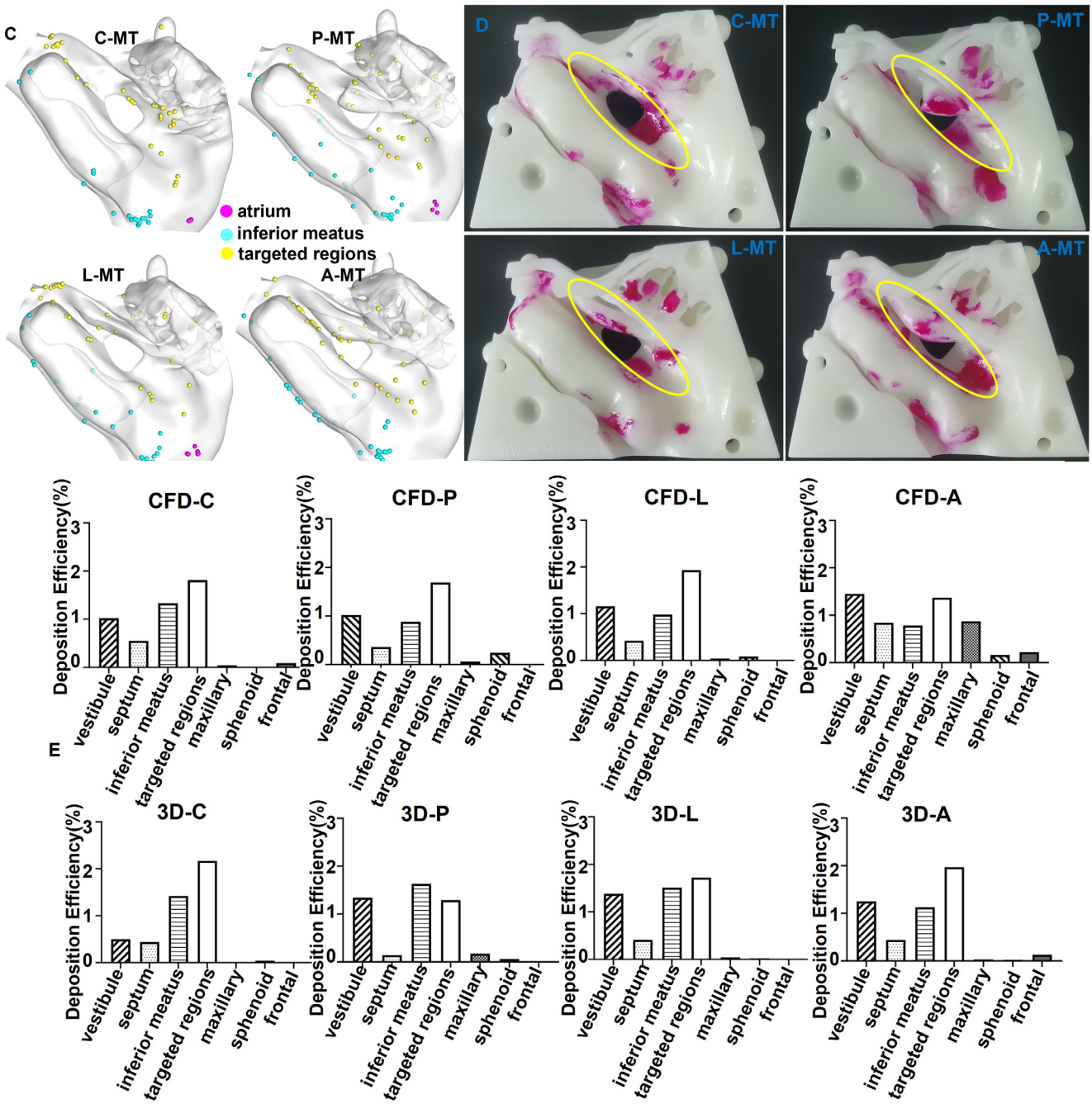

Figure 5 *continued*. Particle deposition in respective MT models. (C) Deposition patterns of budesonide in the CFD simulated models. (D) Deposition patterns of budesonide in the 3D printed models. (yellow: middle turbinate). (E) Comparison between CFD and HPLC data.

septum, and superior turbinate. The airway volume increases, nasal resistance decreases, with more airflow and drug transport to the olfactory region leading to an improved sense of smell [45, 46]. On the other hand, there were significant changes in the regional deposition of nasal medication following different types of MT with varying surgical scopes. The DE of the targeted regions increased following MT, with the greatest deposition following posterior MT in current study. However, it's important to note that MT results in a substantial loss of mucosal surface area, representing an average reduction of 972.86 mm^2 (average accounts for 18.02% of the total mucosal surface area in the targeted region). Prior research has demonstrated that the resection of middle turbinate can lead to a decrease in available mucosal surface area for heat and moisture exchange, leading to a notable reduction in nasal heating and humidification efficiencies [6]. Furthermore, our CFD predictions and HPLC data (Figure 5) provide evidence that, depending on the extent of MT resection, the regional deposition of nasally applied medications experienced notable variations, especially in regions such as the septum, inferior meatus, and the targeted area. In addition,

partial MT may cause middle turbinate drift, nasal mucosal secondary inflammation, adhesion, obstruction, and recurrence in the long term. Empty nose syndrome (ENS) is a rare, late complication of turbinate surgery and it can subsequently cause a high degree of suffering in the patient. It is speculated that anatomical changes leading to alterations in local environment, disruption of mucosal cooling, and disruption of neurosensory mechanisms are strongly implicated [47]. However, the long-term efficacy of MT was not investigated in the current study.

Deposition of the inhaled particles at different sites in the upper and lower respiratory tract is size dependent. Our study confirms prior observations that particles with diameter ≥10 μm may be deposited in the sinus cavities. Smaller particles with less inertia tend to follow the streamlines and bypass the nasal cavity, while larger particles are more likely to deposit within the nasal cavity due to inertial impact. Abouali et al. investigated the effect of maxillary sinus ostium size on particle DE and found that the peak of deposition occurred for particles around 10 μm in a healthy volunteer [48]. The peak of deposition in the maxillary sinus also occurred around 10 μm in the Pre-MT models in the current study. However, the peak of maxillary sinus deposition occurred for particles with diameter >10 μm following MT. Notably, our results identified an ideal aerosol particle size range of 18-26 μm for post-MT deposition via nebulization, this research finding could help to improve the efficacy of targeted therapeutic drug delivery. It is worth noting that, to reduce the model complexity, the effect of particle aggregation during the transport process along the airway was omitted. Based on existing literature, aggregate deposition in the human respiratory system can be described as a function of I) aerodynamic diameter; II) inhaled particle position within the airway system; and III) breathing conditions [49, 50]. Sturm et al. reported that highest deposition values were obtained for nano-scale aggregates (<10 nm), whereas larger aggregates exhibited slightly to significantly reduced deposition probabilities [50]. Meanwhile, for the present study, only nebulized inhalation therapy with water-based solutions was considered as a post-operative care treatment. Therefore, the droplet density was assumed as water density, and the effect of variation in medicine materials was not considered. We also acknowledge that environmental conditions, specifically relative humidity, and temperature, play a role in determining the size of the droplets during their transport through the airway. However, in the context of inhalation therapy, these factors are considered minimal as the relative humidity remains nearly constant at 100% throughout the system.

Limitations

While the study reports certain research findings, it's important to acknowledge that the proposed numerical and experimental modelling approach inherently cannot fully replicate the realistic airflow and particle deposition patterns in the human airway. Several limitations include: I) The model is simplified, where the interactions of nasal hair, nasal mucosal blood vessels, and nerves on drug droplets are not considered; II) The sample size of this study was too small to make statistical inference. Inter-subject differences may affect the results; III) Particles are assumed spherical, where evaporation and condensation of droplets are not considered; IV) Assuming steady-state laminar flow condition, time-dependent flow feature to the deposition in the sinuses need to be further investigated. We intend to address these limitations in future studies.

Conclusion

This study presents a combined numerical and experimental investigation based on six post-FESS nasal samples, which is believed to be the largest sample cohort reported in the literature to date. Quantitative data on drug aerosol deposition in the nasal cavity and paranasal sinuses following different scopes of MT were presented in detail. The findings strongly affirm the vast potential of transnasal nebulization as an effective post-FESS treatment option. Moreover, it emphasizes that the drug delivery process via atomizers to the nasal cavity and paranasal sinuses is highly sensitive to the particle size. The optimal particle size for transnasal atomization in post-MT patients is in the range of 18-26 μm. Heterogeneous particle sizes using this range may be more efficient than single particle sizes.

Abbreviations

A-MT: anterior 1/3 middle turbinectomy; CRS: chronic sinusitis; CRSwNP: chronic sinusitis with nasal polyps; C-MT: complete middle turbinectomy; CFD: computational fluid dynamics; CFPD: computational fluid-particle dynamics; CT: computed tomography; DE: deposition efficiency; DPM: discrete phase model; ENS: empty nose syndrome; FESS: functional endoscopic sinus surgery; HPLC: high-speed liquid chromatography; HU: hounsfield: L-MT: lateral middle turbinectomy; MT: middle turbinectomy; P-MT: posterior middle turbinectomy; Q3: 3rd quartile; WSS: wall shear stress; 3D: three-dimensional.

Authorship contribution

RM: conceptualization, methodology, validation, formal analysis, writing - original draft, writing - review & editing. LT: methodology, writing - review & editing. YW: formal analysis, writing - review & editing. SS: validation, methodology. JZ: collecting data. ML: software, validation, investigation, methodology. ZH: data curation, visualization. MG: investigation, visualization.
FY: validation. GZ: conceptualization, methodology, funding acquisition. JD: conceptualization, methodology, validation, writing - review & editing, funding acquisition. YZ: conceptualization, methodology, validation, formal analysis, funding acquisition.

Conflict of interest

The authors declare that they have no known competing financial interests or personal relationships that could have appeared to influence the work reported in this paper.

Funding

This research was funded by National Natural Scientific Foundation of China [grant number 82000960]; Universities Co-funded Project of Key Research and Development Project of Shaanxi Province [grant number 2020GXLH-Y-017]; and the Science and Technology Planning Project of Yulin City [grant number CXY-2020-047]; and the Australian Research Council [grant number DE180101138 and DE210101549].

This work was performed in part at the Melbourne Centre for Nanofabrication (MCN) in the Victorian Node of the Australian National Fabrication Facility (ANFF). It was supported in part by the MCN Technology Fellow Ambassador program (received by Dr. Jingliang Dong).

References

1. Akiyama K, Samukawa Y, Takahashi S, Ouchi Y, Hoshikawa H. Clinical effects of submucosal middle turbinectomy for eosinophilic chronic rhinosinusitis. Auris Nasus Larynx 2018;45(4):765-71.
2. Soler ZM, Hwang PH, Mace J, Smith TL. Outcomes after middle turbinate resection: revisiting a controversial topic. Laryngoscope 2010;120(4):832-7.
3. Fokkens WJ, Lund VJ, Hopkins C, Hellings PW, Kern R, Reitsma S, et al. European position paper on rhinosinusitis and nasal polyps 2020. Rhinology 2020;58(Suppl S29):1-464.
4. Maza G, Li C, Krebs JP, Otto BA, Farag AA, Carrau RL, et al. Computational fluid dynamics after endoscopic endonasal skull base surgery-possible empty nose syndrome in the context of middle turbinate resection. Int Forum Allergy Rhinol 2019;9(2):204-11.
5. Lee KB, Jeon YS, Chung SK, Kim SK. Effects of partial middle turbinectomy with varying resection volume and location on nasal functions and airflow characteristics by CFD. Comput Biol Med 2016;77:214-21.
6. Dayal A, Rhee JS, Garcia GJ. Impact of middle versus inferior total turbinectomy on nasal aerodynamics. Otolaryngol Head Neck Surg 2016;155(3):518-25.
7. Zhao K, Malhotra P, Rosen D, Dalton P, Pribitkin EA. Computational fluid dynamics as surgical planning tool: a pilot study on middle turbinate resection. Anat Rec (Hoboken) 2014;297(11):2187-95.
8. Friedman M, Caldarelli DD, Venkatesan TK, Pandit R, Lee Y. Endoscopic sinus surgery with partial middle turbinate resection: effects on olfaction. Laryngoscope 1996;106(8):977-81.
9. Lou H, Wang C, Zhang L. Steroid transnasal nebulization in the treatment of chronic rhinosinusitis. Curr Opin Allergy Clin Immunol 2016;16(1):39-44.
10. Farzal Z, Basu S, Burke A, Fasanmade OO, Lopez EM, Bennett WD, et al. Comparative study of simulated nebulized and spray particle deposition in chronic rhinosinusitis patients. Int Forum Allergy Rhinol 2019;9(7):746-58.
11. Wang C, Cheng L, Li H, Liu Z, Lou H, Shi J, et al. Chinese expert recommendation on transnasal corticosteroid nebulization for the treatment of chronic rhinosinusitis 2021. J Thorac Dis 2021;13(11):6217-6229.
12. Kolanjiyil AV, Walenga R, Babiskin A, Golshahi L, Hindle M, Longest W. Establishing quantitative relationships between changes in nasal spray in vitro metrics and drug delivery to the posterior nasal region. Int J Pharm 2023;635:122718.
13. Wang C, Lou H, Wang X, Wang Y, Fan E, Li Y, et al. Effect of budesonide transnasal nebulization in patients with eosinophilic chronic rhinosinusitis with nasal polyps. J Allergy Clin Immunol 2015;135(4):922-9.
14. Zhang Y, Lou H, Wang Y, Li Y, Zhang L, Wang C. Comparison of corticosteroids by 3 approaches to the treatment of chronic rhinosinusitis with nasal polyps. Allergy Asthma Immunol Res 2019;11(4):482-97.
15. Pourmehran O, Arjomandi M, Cazzolato B, Tian Z, Vreugde S, Javadiyan S, et al. Acoustic drug delivery to the maxillary sinus. Int J Pharm 2021;606:120927.
16. Frank DO, Kimbell JS, Pawar S, Rhee JS. Effects of anatomy and particle size on nasal sprays and nebulizers. Otolaryngol Head Neck Surg 2012;146(2):313-9.
17. Siu J, Shrestha K, Inthavong K, Shang Y, Douglas R. Particle deposition in the paranasal sinuses following endoscopic sinus surgery. Comput Biol Med 2020;116:103573.
18. Siu J, Dong J, Inthavong K, Shang Y, Douglas RG. Quantification of airflow in the sinuses following functional endoscopic sinus surgery. Rhinology 2020;58(3):257-65.
19. Ma Z, Kourmatzis A, Milton-McGurk L, Chan HK, Farina D, Cheng S. Simulating the effect of individual upper airway anatomical features on drug deposition. Int J Pharm 2022;628:122219.
20. Tanprasert S, Kampeewichean C, Shiratori S, Piemjaiswang R, Chalermsinsuwan B. Non-spherical drug particle deposition in human airway using computational fluid dynamics and discrete element method. Int J Pharm 2023;639:122979.
21. Wofford MR, Kimbell JS, Frank-Ito DO, Dhandha V, McKinney KA, Fleischman GM, et al. A computational study of functional endoscopic sinus surgery and maxillary sinus drug delivery. Rhinology 2015;53(1):41-8.
22. Williams J, Kolehmainen J, Cunningham S, Ozel A, Wolfram U. Effect of patient inhalation profile and airway structure on drug deposition in image-based models with particle-particle interactions. Int J Pharm 2022;612:121321.
23. Inthavong K, Chetty A, Shang Y, Tu J. Examining mesh independence for flow dynamics in the human nasal cavity. Comput Biol Med 2018;102:40-50.
24. CMK Se, Inthavong K, Tu J. Unsteady particle deposition in a human nasal cavity during inhalation. J Comput Multiph Flows 2010;2:207-218.
25. Kuprat AP, Price O, Asgharian B, Singh RK, Colby S, Yugulis K, et al. Automated bidirectional coupling of multiscale models of aerosol dosimetry: validation with subject-specific deposition data. J Aerosol Sci 2023;174:106233.
26. Bahmanzadeh H, Abouali O, Faramarzi M, Ahmadi, G. Numerical simulation of airflow and micro-particle deposition in human nasal airway pre- and post-virtual sphenoidotomy surgery. Computers in Biology and Medicine 2015;61:8-18.
27. Isabey D, Chang HK. Measurement of flow velocities in a central airway model. Federation Proceedings 1981;40(3):596.
28. Bahmanzadeh H, Abouali O, Ahmadi G. Unsteady particle tracking of micro-particle deposition in the human nasal cavity under cyclic inspiratory flow. Journal of Aerosol Science 2016;101:86–103.
29. Kelly J, Prasad A, Wexler A. Detailed flow patterns in the nasal cavity. J Appl Physiol 2000;89:323–337.
30. Keyhani K, Scherer PW, Mozell MM. A numerical model of nasal odorant transport for the analysis of human olfaction. J Theor Biol 1997;186:279–301.
31. Zhao K, Jiang J. What is normal nasal airflow? A computational study of 22 healthy adults. Int Forum Allergy Rhinol 2014;4(6):435-46.
32. Brandon BM, Austin GK, Fleischman G, Basu S, Kimbell JS, Shockley WW, et al. Comparison of airflow between spreader grafts and butterfly grafts using computational flow dynamics in a cadaveric model. JAMA Facial Plast Surg 2018;20(3):215-21.
33. Li L, Han D, Zhang L, Li Y, Zang H, Wang T, et al. Impact of nasal septal perforations of varying sizes and locations on the warming

function of the nasal cavity: a computational fluid-dynamics analysis of 5 cases. Ear Nose Throat J 2016;95(9):E9–e14.
34. Lou M, Zhang L, Zhang J, Ma R, Gong M, Hu Z, et al. Numerical simulation of nasal airflow aerodynamics, and warming and humidification in models of clival chordoma pre- and post-endoscopic endonasal surgery. Respir Physiol Neurobiol 2021;291:103693.
35. Shang Y, Dong J, Inthavong K, Tu J. Comparative numerical modeling of inhaled micron-sized particle deposition in human and rat nasal cavities. Inhal Toxicol 2015;27:694–705.
36. Ounis H, Ahmadi G, McLaughlin JB. Brownian diffusion of submicrometer particles in the viscous sublayer. J Colloid Interface Sci 1991;143:266–277.
37. Jain R, Kumar H, Tawhai M, Douglas R. The impact of endoscopic sinus surgery on paranasal physiology in simulated sinus cavities. Int Forum Allergy Rhinol 2017;7(3):248-55.
38. Hu Z, Dong J, Lou M, Zhang J, Ma R, Wang Y, et al. Effect of different degrees of adenoid hypertrophy on pediatric upper airway aerodynamics: a computational fluid dynamics study. Biomech Model Mechanobiol 2023;22(4):1163-1175.
39. Schroeter JD, Garcia GJ, Kimbell JS. Effects of surface smoothness on inertial particle deposition in human nasal models. J Aerosol Sci 2011;42(1):52-63.
40. Kundoor V, Dalby RN. Assessment of nasal spray deposition pattern in a silicone human nose model using a color-based method. Pharm Res 2010;27(1):30-6.
41. Albu S. Novel drug-delivery systems for patients with chronic rhinosinusitis. Drug Des Devel Ther 2012;6:125-32.
42. Brescia G, Pavin A, Giacomelli L, Boninsegna M, Florio A, Marioni G. Partial middle turbinectomy during endoscopic sinus surgery for extended sinonasal polyposis: short- and mid-term outcomes. Acta Otolaryngol 2008;128(1):73-7.
43. Mariano FC, Hamerschmidt R, Soares C, Moreira AT. The middle turbinate resection and its repercussion in olfaction with the University of Pennsylvania smell identification test (UPSIT). Int Arch Otorhinolaryngol 2018;22(3):280-3.
44. Apuhan T, Yildirim YS, Simsek T, Yilmaz F, Yilmaz F. Concha bullosa surgery and the distribution of human olfactory neuroepithelium. Eur Arch Otorhinolaryngol 2013;270(3):953-7.
45. Alam S, Li C, Bradburn KH, Zhao K, Lee TS. Impact of middle turbinectomy on airflow to the olfactory cleft: A computational fluid dynamics study. Am J Rhinol Allergy 2019;33(3):263-8.
46. Zhao K, Jiang J, Pribitkin EA, Dalton P, Rosen D, Lyman B, et al. Conductive olfactory losses in chronic rhinosinusitis? A computational fluid dynamics study of 29 patients. Int Forum Allergy Rhinol 2014;4(4):298-308.
47. Kuan EC, Suh JD, Wang MB. Empty nose syndrome. Curr Allergy Asthma Rep 2015;15(1):493.
48. Abouali O, Keshavarzian E, Farhadi GP, Faramarzi A, Ahmadi G, Bagheri MH. Micro and nanoparticle deposition in human nasal passage pre and post virtual maxillary sinus endoscopic surgery. Respir Physiol Neurobiol 2012;181(3):335-45.
49. Sturm R. Theoretical deposition of carcinogenic particle aggregates in the upper respiratory tract. Ann Transl Med 2013;1(3):25.
50. Muralidharan P, Malapit M, Mallory E, Hayes D, Mansour H. Inhalable nanoparticulate powders for respiratory delivery. Nanomedicine-UK 2015;11(5):1189-99.

Ya Zhang
Department of Otolaryngology
Head and Neck Surgery
The Second Affiliated Hospital of
Xi'an Jiaotong University
157 Xiwu Road
Xi'an
Shaanxi
710000, China

Tel: +86-15102966990
E-mail: zhangya@xjtu.edu.cn

Guoxi Zheng
Department of Otolaryngology Head
and Neck Surgery
The Second Affiliated Hospital of
Xi'an Jiaotong University
157 Xiwu Road
Xi'an
Shaanxi
710000, China

Tel: +86-13509186588;
E-mail: zhengguoxi888@sina.com

Jingliang Dong
Institute for Sustainable Industries &
Liveable Cities
Victoria University
PO Box 14428
Melbourne
VIC 8001
Australia

First Year College
Victoria University
Footscray Park Campus
Footscray
VIC 3011
Australia

Tel: +61-3-9919-5622
E-mail: jingliang.dong@vu.edu.au